Progress in Earth and Planetary Science

REVIEW

Open Access

Enstatite chondrites: condensation and metamorphism under extremely reducing conditions and contributions to the Earth

Yangting Lin*

Abstract

Enstatite chondrites are a small clan of meteorites, only ~ 1% out of all meteorite collection. However, they are the most reduced meteorites and have almost identical isotopic compositions to those of the Earth, suggestive of significant contributions to the latter and other terrestrial planets. Enstatite chondrites contain a unique mineral inventory of sulfides of typical lithophile elements, Si-bearing metal, silicide and phosphide, which record the nebular processes and the thermal metamorphism in asteroidal bodies under extremely reducing environments. EH group is mainly characteristic of the higher Si content of metallic Fe–Ni and the higher MnS contents of sulfides than EL group, indicative of a more reducing condition than the latter. However, the fugacity p_{H2S} could be the same in both EH and EL regions, because it was buffered by kamacite and troilite. The majority of sulfides condensed from the nebula, partially enclosing schreibersite micron-spherules formed probably by early melting. Another part of troilite, sphalerite and djerfisherite, intergrown with perryite, were produced via sulfidation of metallic Fe–Ni. Minor exotic components were also found in enstatite chondrites, including Ca-, Al-rich inclusions and FeO-rich silicate clasts. The Ca-, Al-rich inclusions are identical to those in carbonaceous chondrites except for the alteration under reducing environments, and the FeO-rich silicate clasts show reduction reactions, both suggestive of migration of dust in the protoplanetary disk. The highly reducing conditions (as C/O ratios) might be established via repeating evaporation and condensation of water ice and organic matter across the snow line along the protoplanetary disk, but need to find evidence. Another issue is the preservation of submicron-to-micron-sized presolar grains during high-temperature condensation of the major constituent minerals. After accretion, the parent bodies of EH and EL chondrites probably experienced distinct thermal histories, indicated by their distinct petrologic-type distributions and different correlations with the closure temperatures determined by the FeS contents of sulfides in contact with troilite.

Keywords: Enstatite chondrite, Condensation of the solar nebula, Reducing conditions, Inner solar system, Building blocks of the Earth

1 Classification

1.1 Chemical groups and petrographic types

Chemical groups: Enstatite chondrites are a small clan of chondrites (~ 1%) (Meteoritical Bulletin Database, 2021), characteristic of a unique mineral inventory, including FeO-poor enstatite, Si-bearing metallic Fe–Ni and various sulfides of typical lithophile elements (e.g., K, Na, Mg, Ca, Mn and Cr). This unique mineral inventory indicates highly reducing conditions. Enstatite chondrites were classified as types I, intermediate and II, with type I referred to unequilibrated and type II to highly recrystallized (Keil 1968). Later, types I and intermediate were re-designated as EH (high-Fe) and Type II as EL (low-Fe) groups, following the classification scheme of H and L groups of ordinary chondrites (Sears et al., 1982). Besides EH and EL chondrites, a few of enstatite chondrites were

*Correspondence: LinYT@mail.iggcas.ac.cn

Institute of Geology and Geophysics, Chinese Academy of Sciences, Beijing 100029, China

anomalous, with a part of them classified as an intermediate grouplet based on their mineral compositions plotted between EH and EL (Lin and Kimura 1998). It is noted that most of the anomalous enstatite chondrites are highly recrystallized due to impact melting or thermal metamorphism.

Petrologic types: Before the classification of MAC 88136 as the first EL3 (Lin et al. 1991), all EL chondrites were highly recrystallized and classified as EL6, whereas EH chondrites ranged from EH3 to EH5. Although Reckling Peak A80259 was reported as the first EL5 (Sears et al. 1984), it contains niningerite and high Si content of metallic Fe–Ni (Sears et al. 1984), typical of EH group. This meteorite was later assigned as EH5 (Meteoritical Bulletin Database). Both EHs and ELs consisted of an apparent continuum of petrographic types from EH3-5 to EL6, implying origination from a same parent body. However, the discovery of the EL3 MAC 88136 supplies with robust evidence for separate thermal metamorphism sequences of EH and EL groups (Lin et al. 1991). With more collection of enstatite chondrites (a total of ~ 400), EH and EL groups display distinct patterns of petrographic types, with EHs (184) dominated by type 3 (from type 3 to 6: 75.4%, 15.8%, 3.9%, 4.9%), while ELs (177) by type 6 (from type 3 to 6: 14.1%, 10.7%, 5.1%, 70.1%) (Meteoritical Bulletin Database, 2021). In addition, melt rocks (probably impact-induced) are common in both EHs (8%) and ELs (11.5%). The distinct distribution patterns of petrographic types between EHs and ELs suggest different thermal histories and internal structures of their parent bodies.

1.2 Taxonomic parameters

Following the Van Schmus–Wood two-dimensional classification scheme (Van Schmus and Wood 1967), EHs were designated to high-Fe enstatite chondrites with higher abundances of metallic Fe–Ni and total Fe, whereas ELs to those with low-Fe (Keil 1968; Sears et al. 1982). However, studies of more enstatite chondrites demonstrated a wide range of metallic Fe–Ni abundances, which overlap between EH3s (4.1–13.4 vol%) and EL3s (9.4–10.7 vol%) (Weisberg and Kimura 2012). The wide range of modal abundance of metallic Fe–Ni could be attributed to heterogeneous sampling; hence, it is not a key parameter to distinguish EHs from ELs. Instead, mineral chemistry preserves the different forming conditions of EH and EL parent bodies.

Si contents of metallic Fe–Ni: The Si contents of metallic Fe–Ni are distinguishably higher in EHs (> 1.9 wt% Si) than in ELs (< 1.8 wt% Si) (Fig. 1). EH and EL groups show significant overlapping of the Ni contents of metallic Fe–Ni, but both EH3s and EL3s intend to contain Ni-poor metallic Fe–Ni than the equilibrated and/or impact melts, respectively (Fig. 1). It is noticed that the metallic Fe–Ni in the anomalous enstatite chondrites Y793225 and Itqiy show a wide range of Si contents covering both EHs and ELs (Fig. 1), and Y793225 was designated as the intermediate grouplet (Lin and Kimura 1998). Consistent with the higher Si content of metallic Fe–Ni in EHs, perryite ($(Ni, Fe)_5(Si, P)_2$), a common minor silicide in enstatite chondrites, is more abundant in EH3s (average 0.8 vol%, range 0.4–1.3 vol%) than in EL3s (average 0.1 vol%, range < 0.1–0.4 vol%) (Weisberg and Kimura 2012). Furthermore, perryite also contains higher Si in EHs (11.9–13.4 wt% Si) than that in ELs (10.4–11.2 wt% Si) (Lin and El Goresy 2002).

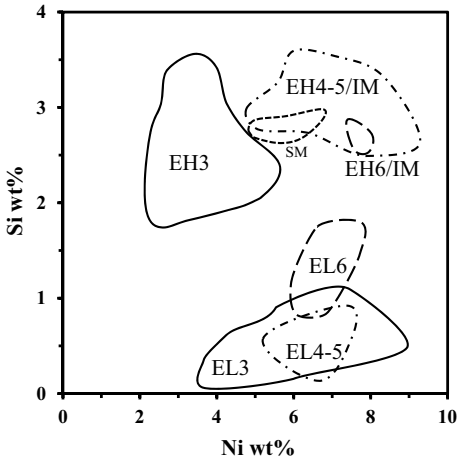

Fig. 1 The Si and Ni contents of metallic Fe–Ni from enstatite chondrites. Abbreviation: SM-St. Marks, IM—impact melt. Data from (Lin and Kimura 1998; Patzer et al. 2001, 2004; Lin and El Goresy 2002; Kimura et al. 2005; Rubin and Wasson 2011; Weisberg and Kimura 2012; Horstmann et al. 2014; Weyrauch et al. 2018)

Presence of niningerite or alabandite: Another critical difference between EHs and ELs is the composition of (Mg, Fe, Mn)S solid solution, which is referred to as niningerite (Mg-predominant, Mg > Mn) in EHs, whereas as alabandite (Mn-predominant, Mn > Mg) in ELs (Fig. 2). The FeS contents of both niningerite and alabandite were mainly determined by equilibrium with troilite, increasing with temperature (Skinner and Luce 1971). The presence of alabandite in ELs cannot be a result of thermal metamorphism of niningerite, which has been demonstrated by the presence of alabandite in MAC 88136 (Lin et al. 1991) and other EL3 chondrites (Weisberg and Kimura 2012). As shown in Fig. 2, niningerite within individual EHs plots parallel to the MgS–FeS joint line with the constant MnS contents. The homogeneous MnS contents of niningerite within the individual meteorites have also been demonstrated by the zoning profiles conducted on the Qingzhen EH3 chondrite, which show

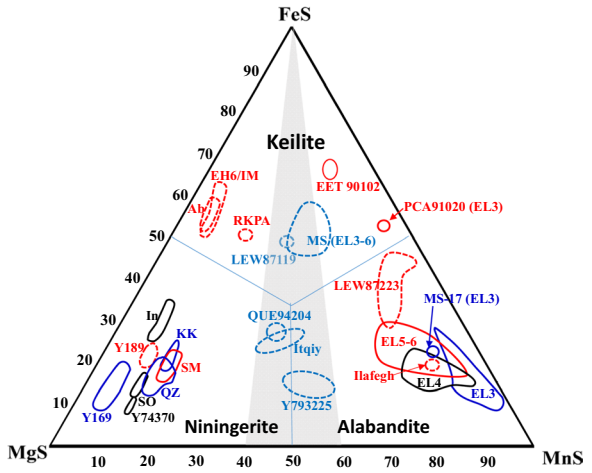

Fig. 2 MgS–MnS–FeS diagram of (Mg, Mn, Fe)S solid solution from enstatite chondrites. Dashed lines are impact melt (IM). Abbreviation: KK—Kota-Kota (EH3), QZ—Qingzhen (EH3), Y169 (EH3), In—Indarch (EH4), SO—South Oman (EH4), Y74370 (EH4), SM—St. Marks (EH5), Y189—Y82189 (EH IM), RKPA—RKPA 80259 (IM), Ab—Abee (EH IM); EH6/IM including Y8404, Y980211, Y980223, LEW 88180; Grein 002 (EL4), LEW 87223 (EL IM), Ilafegh–Ilafegh 009 (EL IM); LEW 87119 (EL6, IM); MS (EL3-6) including MS-7 (EL5/6), 52 (EL6), 159 (EL6), 196 (EL5), 200 (EL3/4), MS-D (EL6) and MS-MU003 (EL3/4); Data from (Zhang et al. 1995; Fogel 1997; Lin and Kimura 1998; Patzer et al. 2001, 2004; Lin and El Goresy 2002; Keil 2007; Rubin and Wasson 2011; Weisberg and Kimura 2012; Weyrauch et al. 2018)

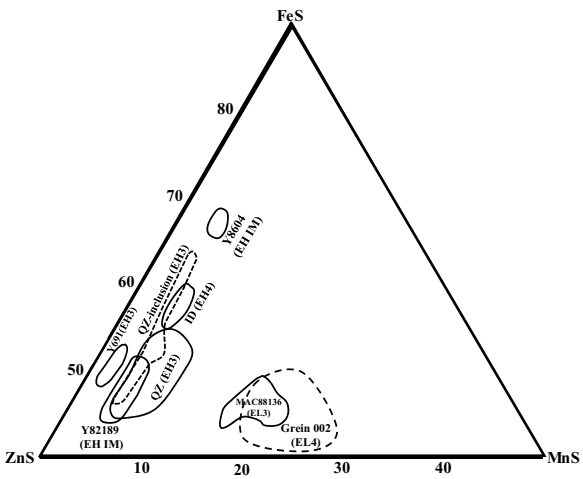

Fig. 3 ZnS–FeS–MnS content ranges of sphalerite from enstatite chondrites. Abbreviation: QZ—Qingzhen, IM—impact melt. Data from (El Goresy et al. 1988; Nagel et al. 1989; Lin and Kimura 1998; Lin and El Goresy 2002; Patzer et al. 2004)

the constant MnS contents regardless of variation in the FeS and MgS contents (Lin and El Goresy 2002). For alabandite in ELs, it shows constant or small variation in the MgS contents. Hence, the presence of niningerite can be referred to as the diagnostic parameter for EHs, and alabandite for ELs. A part of the (Mg, Fe, Mn)S solid solution contain higher FeS than MgS and MnS, which was named as keilite (Keil 2007). The keilite-bearing enstatite chondrites are usually highly recrystallized or melt rocks. In addition, a few of enstatite chondrites have an intermediate Mg/Mn ratio of the (Mg, Fe, Mn)S solid solution and plot between niningerite and alabandite (Fig. 2). They were referred to as the intermediate grouplet (Lin and Kimura 1998), including LEW 87119, QUE 94204, Itqiy and Y-793225. It is also noticed that a number of enstatite chondrite clasts of Almahata Sitta classified as EL3-6 (Weyrauch et al. 2018) also have the intermediate compositions of the (Mg, Mn, Fe)S solid solution (Fig. 2), which is consistent with their higher Mn contents of troilite than those of typical EHs (Weyrauch et al. 2018).

Mn contents of sulfides: The Mn/Mg ratios of other sulfides also show systematic differences between EHs and ELs, consistent with the presence of niningerite in EHs and alabandite in ELs. Figure 3 plots the compositions of sphalerite, with the MnS content significantly higher in ELs than those in EHs. Furthermore, sphalerite grains within and among EH chondrites show variation parallel to the FeS–ZnS joint line, suggestive of relatively constant MnS contents. The relatively constant MnS content of sphalerite is remarkable in Qingzhen, with the sphalerite inclusions in kamacite varying in a wide range of the FeS content. In addition, the FeS contents tend to correlate with the petrographic type, with an exception of Y-82189 impact melt overlapping EH3s (Fig. 3). These variations are similar to those of niningerite described above. Daubréelites contain higher Zn and lower Mn in EHs (up to 10 wt% Zn, < 1.4 wt% Mn) than those in ELs (< 4 wt% Zn, 0.8–4.0 wt% Mn) (Keil 1968; Lin and El Goresy 2002), although partly overlapping between both groups. These systematic differences in the Mn/Mg ratios of sulfides between EHs and ELs could not be attributed solely to buffering of niningerite or alabandite. Oldhamite contains minor Mg, Mn and Fe. It probably predated niningerite in EHs and alabandite in ELs, based on its higher REE concentrations (Lodders and Fegley 1993; Crozaz and Lundberg 1995) and higher condensation temperature than the latter (Lattimer and Grossman 1978; Fegley 1982; Lodders and Fegley 1993). The Mn/Mg ratio of oldhamite is also significantly higher in the EL3 Almahata Sitta (~ 1.3) (El Goresy et al. 2017) than that of the EH3 Qingzhen (~ 0.14) (Lin and El Goresy 2002). Hence, the higher MnS contents of sulfides in ELs than EHs were established from the beginning of condensation.

2 Initial status of the innermost protoplanetary disk

2.1 Low temperature for preserving presolar grains

Noble gas analysis of the acid residues from primitive EHs indicated the presence of presolar diamond and SiC (Huss and Lewis 1995). The presolar diamond is a few nm in size and separated from the acid residue as colloid (Lewis et al. 1987; Lin et al. 2002a), and the majority of presolar SiC is submicron to micron in size (Lin et al. 2002a). Hence, the presence of presolar grains is very sensitive to thermal metamorphism. In fact, the abundance of presolar grains drops fast with the petrographic types (Huss and Lewis 1995). Separation and analysis of the presolar grains from the Qingzhen EH3 reveal various types of presolar SiC and Si_3N_4 grains, including X grains, type AB and Main Stream, with the relative abundance ratios and the size distribution pattern similar to those separated from carbonaceous chondrites (Lin et al. 2002a, 2010). Presolar graphite was also identified in the acid residue from Qingzhen, with similar morphologies and isotopic compositions of those from the CM2 Murchison (Xu et al. 2016, 2018). Furthermore, presolar silicate grains were found in EH3s by in situ isotope mapping (Zhao et al. 2010).

The presence and high abundance of presolar grains in EH3s indicate that the temperature at enstatite chondrite-accreting regions has never been entirely heated up to a maximum temperature of 440 ℃, otherwise the nano-sized diamond and submicron-sized SiC would have been largely destroyed (Davidson et al. 2014). On the other hand, the majority of the constituent minerals condensed from the nebular gas at high temperature. For instant, oldhamite condensed from the reducing nebula at > 1000 K (Larimer and Bartholomay 1979), and at least a part of troilite and sphalerite condensed at a temperature ~ 700 K (Lin et al. 2002a), both are too high to preserve the presolar grains. This discrepancy requires that enstatite chondrites accreted with materials condensed in hot zones and the presolar dusts preserved separately in cold regions. The presolar grains were probably transported from the outer cold zones or dropped from the cold periphery of the protoplanetary disk to the midplane, where the unique constituent minerals condensed under highly reducing conditions and enstatite chondrite parent bodies finally accreted. However, the scenario that presolar grains delivered from the outer solar system is inconsistent with the high abundances of presolar SiC and diamond in Qingzhen (Lin et al. 2002a), which are comparable with those in primitive carbonaceous chondrites. Boyet et al. (2013) analyzed Nd isotopes in primitive enstatite chondrites. They found the largest ^{142}Nd excess in ALHA77295 even than the CM2 Murchison, which is attributed to presolar SiC as the major carrier. Another argument against this scenario is that few carbonaceous chondrite components have been identified in primitive enstatite chondrites. Zhu et al. (2020) reported two chondrules from the EH3 Sahara 97096 with definitely ^{54}Cr-anomaly (ε up to 1.01± 0.11) within the range of carbonaceous group. Alternatively, the majority of minerals (except for the presolar grains) condensed probably very close to the Sun and then transported outward to the regions where enstatite chondrites accreted altogether with the presolar grains preserved at low temperature.

In summary, the presence and abundance of submicron-sized presolar grains in primitive enstatite chondrites provide robust evidence for a low temperature in enstatite chondrite-accreting regions of the protoplanetary disk. However, this discovery conflicts with the high-temperature condensation of enstatite chondrites, which took place under extremely reducing conditions in the regions probably closest to the proto-Sun as discussed below. This discrepancy should be addressed by formation and evolution models of the solar nebula.

2.2 Extremely low fO_2

The predominant FeO-poor enstatite and the unique opaque minerals in enstatite chondrites demonstrate highly reducing environments. In EH3 chondrites, there are some FeO-bearing silicate clasts, which appear as dusty grains under optic microscope because of the presence of numerous tiny Ni-free metallic Fe particles (Rambaldi et al. 1984; Lin et al. 2002b). This discovery indicates that the dusty FeO-bearing silicates were exotic, transported from other oxidizing regions and reduced in enstatite chondrite-accreting regions.

The Si contents of metallic Fe–Ni are indicative of the oxygen fugacity of enstatite chondrites. The systematically higher Si contents of metal from EH3s than those from EL3s suggest that the minerals condensed at even lower fO_2 in EH region than in EL's. The more reducing condition of EHs is consistent with the presence of niningerite and lower Mn/Mg ratios of other sulfides, in comparison with the presence of alabandite and higher Mn/Mg ratios of sulfides in ELs. Mg is a typical lithophile element, and Mn behaves more sulfophile. Hence, the MnS/MgS fugacity ratio is sensitive to the redox conditions, decreasing (mainly due to increasing p_{MgS} more than P_{MnS}) in more reducing environments.

The reducing conditions of the solar nebula may be achieved by increasing the C/O ratio from the solar value of 0.52 up to > 0.8–1.0 (Larimer and Bartholomay 1979). However, how and when were the C/O ratios of enstatite chondrite-forming regions enhanced from the canonical values to > 0.8–1.0? A scenario is that repeating processes of condensation and evaporation of water ice and

carbonaceous materials across the snow line (~2.8 AU from the Sun) could play a key role for the evolution of redox along the protoplanetary disk. The water ice and organic solid particles radially migrated inward and were heated and evaporated in the inner solar nebular regions across the snow line. The organic macromolecular matter retained as solid, whereas water ice and small organic molecule materials evaporated. The vapor of water and small organic molecules then diffused to all directions and re-condensed beyond the snow line. Repeating these processes, the C/O ratio of the protoplanetary disk could be enhanced toward the Sun. This scenario is consistent with the redox status of the planets, which appears more reducing closer to the Sun as indicated by the lower FeO contents of silicates and the higher average density (related to the metallic Fe–Ni core/silicate volume ratio). The remote sensing of Mercury revealed the most reducing features of the planets, which are comparable with enstatite chondrites (Vilas 1985; Nittler et al. 2011).

2.3 Buffered fH_2S

The modal abundance of sulfides is higher in EH3s than EL3s (Weisberg and Kimura 2012), indicative of a higher bulk abundance of sulfur in the former and the latter. Furthermore, the perryite–sulfide intergrowth is also more developed in EH3s than EL3s, with metallic nodules commonly surrounded by perryite–sulfide intergrowth rims in EH3s but rather rare in E3Ls as depicted in the next section (Fig. 5). The fugacity of H_2S might be higher when sulfides started to condense in EH-forming region than that in EL's, because of its higher bulk abundance of sulfur. However, the fugacity of H_2S would be buffered in both EH- and EL-forming regions, when troilite started to condense. After condensation of troilite, the H_2S fugacity in the nebular gas was buffered by kamacite and troilite as follows:

$$\text{Kamacite} + H_2S\,(g) = \text{troilite} + H_2(g)$$

where the activities of Fe in kamacite and troilite and the fugacity of H_2 were constant at given temperature.

3 Processes in the reducing nebular regions

3.1 Gas–solid condensation of sulfides

Besides the Si-bearing metal and FeO-poor enstatite, the majority of various sulfides in enstatite chondrites formed likely via gas–solid condensation in highly reducing environments. The key lines of evidence for condensation are as follows:

Mineral compositions: Oldhamite and niningerite in EH3s are usually euhedral and coarse-grained in morphology and commonly present in the centers of opaque mineral assemblages, indicative of early growth in a free space. This is consistent with the condensation calculations, which predicted oldhamite and niningerite as the first two sulfides deposited from the nebula under extremely reducing conditions with C/O ratio $\geq$ 0.8 (Larimer and Bartholomay 1979). Another critical line of evidence for condensation is the high enrichment of REE and other refractory elements in oldhamite and partly in niningerite. SIMS analyses of oldhamite in both EH3s and EL3s revealed highly REE-enriched patterns (~10–100 × CI) w/o anomalies of Eu and Yb (Crozaz et al. 2003; El Goresy et al. 2017), which are consistent with condensation of REE under reducing conditions (Larimer and Ganapathy 1987; Lodders and Fegley 1993). In addition, the normal FeS-zoning profiles were found in niningerite grains from Qingzhen, with the FeS content decreasing from 17.5 mol% at the cores to 15.4 mol% at the rims in contact with silicates or oldhamite (Lin and El Goresy 2002). These normal zonings of niningerite recorded the growth of the grains as temperature decreasing, a process of gas–solid condensation but against sulfidation of silicate grains.

Schreibersite micron-spherules enclosed in sulfides: Two types of schreibersite were reported in enstatite chondrites (Fig. 4), i.e., (1) large grains (up to hundreds μm) in kamacite, and (2) micron-spherules (< 10 μm in diameter) entrapped as inclusions in various sulfides. The coarse-grained schreibersite was enclosed in kamacite usually without coexisting with other minerals. In contrast, the schreibersite micron-spherules enclosed in various sulfides share similar shapes, sizes and compositions, regardless the wide compositional range of the host minerals (e.g., oldhamite, niningerite/alabandite, djerfisherite, sphalerite, minerals A and B, caswellsilverite, daubréelite and troilite). Furthermore, the composition of micron-spherule schreibersite is similar to those of the coarse grains enclosed in kamacite (Lin and El Goresy 2002), indicative of a same origin except that the micron-spherules experienced melting before entrapped by the sulfides. The presence of schreibersite micron-spherules in various sulfides suggests that schreibersite predated all sulfides and the micron-spherules served as nuclei for condensation of the latter. The early formation of schreibersite is supported by the occurrence of the coarse-grained schreibersite in metallic Fe–Ni. Lehner et al. (2010) analyzed trace elements of schreibersite and the host kamacite in the Sahara 97072 EH3 chondrite, and suggested that schreibersite condensed in a reducing gas followed by incorporation into metallic Fe–Ni. Hsu (1998) reported schreibersite micron-spherules in oldhamite, but proposed that they formed via melting of oldhamite with coexisting schreibersite. However, this scenario cannot explain the same occurrence of schreibersite micron-spherules in all types of sulfides, whereas no coexistence of non-melted schreibersite with sulfides.

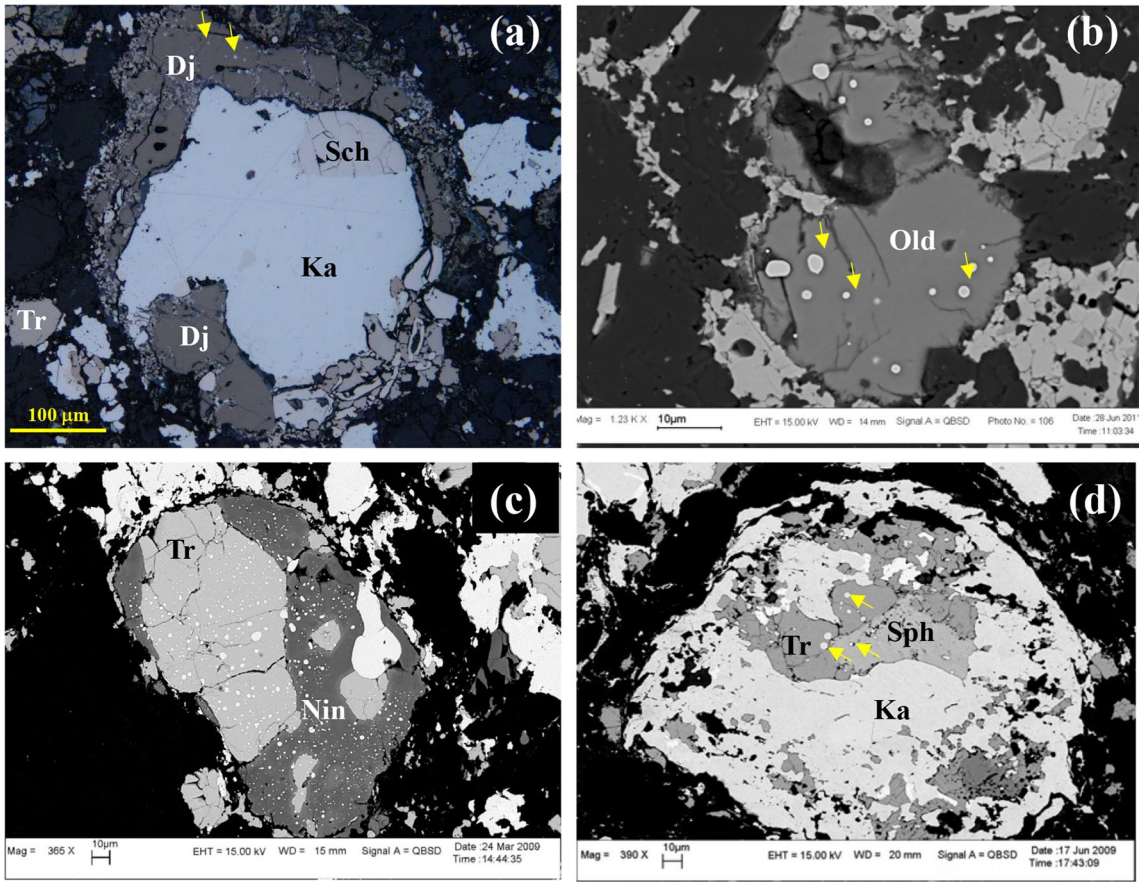

Fig. 4 Occurrences of schreibersite (Sch) in EH3s. **a** A large grain enclosed in kamacite (Ka) and numerous micron-spherules (arrows) enclosed in djerfisherite (Dj) in Qingzhen; **b** small spherules in an oldhamite (Old) fragment in Almahata Sitta MS-17; **c** abundant schreibersite micron-spherules in troilite and niningerite in Sahara 97159; **d** the micron-spherules in troilite and sphalerite in the center of metal-rich nodule in Sahara 97159. Note a mantle enriched in fine-grained troilite and silicates (dark)

Another convincing line of evidence for the gas–solid condensation of sulfides entrapping schreibersite micron-spherules is their systematically different morphology and mineral chemistry in comparison with those intergrown with perryite, which is discussed in the next subsection in detail. Two major occurrences of troilite, sphalerite and djerfisherite were found in EH3s, one entrapping schreibersite micron-spherules depicted here and the other intergrown with perryite. Similar to oldhamite, niningerite and various Cr sulfides, the schreibersite micron-spherule-bearing troilite, sphalerite and djerfisherite are typical of coarse-grained and euhedral, consistent with gas–solid condensation. Furthermore, these troilite and sphalerite grains are highly Ni-depleted (Lin and El Goresy 2002), with Ni/Fe atomic ratios down to $< 10^{-5}$ determined by SIMS (Lin et al. 2011). These grains are the best candidates to detect possible existence of the short-lived ^{60}Fe (Lin et al. 2011). Such Ni depletion is expected for the schreibersite micron-spherule-bearing troilite and sphalerite, which condensed at much lower temperatures (~ 700 K) than metallic Fe–Ni (~ 1350 K) and almost all Ni had deposited into metallic Fe–Ni.

Oldhamite and niningerite in EHs were mainly found as coarse-grained mineral fragments scattered in silicate matrix. In opaque assemblages, both of them usually occur in the centers, suggestive of predating other sulfides. The large fragments of troilite, sphalerite and djerfisherite usually have euhedral shapes. As mentioned above, these troilite, sphalerite and djerfisherite commonly contain schreibersite micron-spherules. Chromium sulfides are daubréelite, caswellsilverite, mineral A and B (El Goresy et al. 1988), and a new aqueous Fe–Cr sulfide (Lin et al. 1990). Except for the new aqueous Fe–Cr sulfide exclusively enclosed in metallic Fe–Ni in Qingzhen (Lin et al. 1990), all other Cr sulfides coexist often with troilite scattering in silicate materials or on the peripheries of metal–sulfide nodules, suggestive of later condensation probably after troilite.

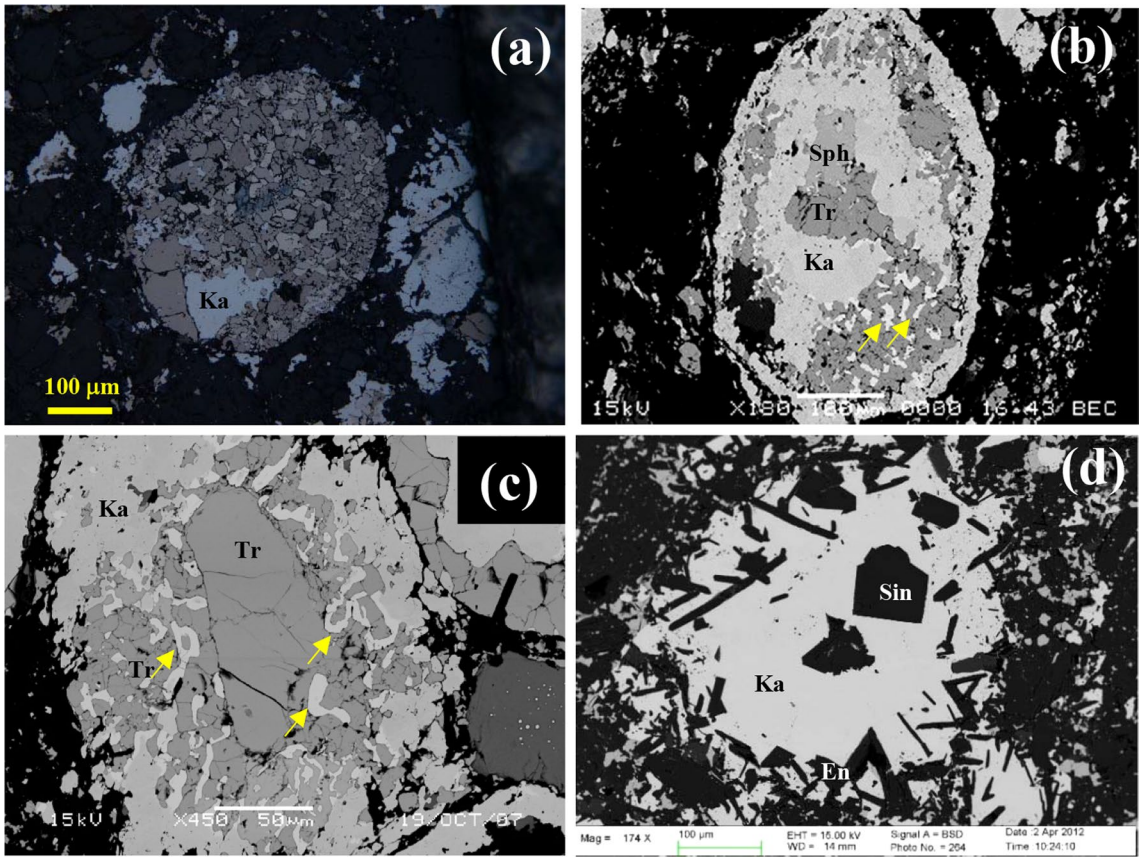

Fig. 5 Intergrowth of kamacite (Ka), perryite (Per) and sulfide in EH3s. **a** A opaque nodule consisting mainly of the intergrown troilite (yellow brown) and perryite (light yellow) in Qingzhen under reflection light; **b** fine-grained troilite (Tr) intergrown with perryite (arrows) in the margin of a nodule from Sahara 97159; **c** the fine-grained troilite intergrown with perryite, note a coarse-grained troilite in the center of the nodule from Sahara 97159; **d** the absence of sulfide and perryite in a metal nodule from Almahata Sitta EL3. Euhedral grains of sinoite (Sin) are enclosed in metal, and enstatite (En) crystals intergrown with metal along the periphery

3.2 Sulfidation of metal

Perryite is a minor phase in enstatite chondrites and shows a common textural occurrence as elongated irregular grains along the boundaries between metal and sulfides (Rambaldi et al. 1986; Lin and El Goresy 2002). In case of the absence of metal, there are only perryite and sulfides intergrown with each other (Lin and El Goresy 2002). It is noticed that the sulfide–perryite intergrowth occurs along the periphery of opaque assemblages and develops inward (Fig. 5). Only troilite, sphalerite and djerfisherite were found to intergrow with perryite (Lin and El Goresy 2002). These perryite-intergrown sulfides are typical of small and irregular, distinguished from those with schreibersite micron-spherules described above. On the other hand, the schreibersite micron-spherule-bearing sulfides usually do not intergrow with perryite, even enclosed in metal. Except for troilite, sphalerite and djerfisherite, all other sulfides including oldhamite, niningerite (in EHs) or alabandite (in ELs), Cr sulfides (daubréelite, caswellsilverite, minerals A and B, and the new aqueous Fe–Cr–S), do not coexist with perryite, and they could contact directly with metal without perryite rims along the interfaces with sulfides. These observations indicate that the perryite-intergrown troilite, sphalerite and djerfisherite were produced by sulfidation of metallic Fe–Ni. The sulfidation reaction took place from the peripheries of metal grains and developed inward. The reaction temperature was about ~ 700 K, based on the thermometer of sphalerite (Lin and El Goresy 2002). With sulfidation, the concentrations of Ni and Si in the metal increased, with perryite nucleating along the boundaries in contact with the sulfides. This scenario is also convincingly supported by the Ni-bearing compositions of the perryite-intergrown troilite and sphalerite (Lin and El Goresy 2002), distinguishing from the highly Ni-depleted grains enclosing schreibersite inclusions discussed above. The distinctly higher Ni contents of the sulfides can be attributed to the enhanced

Ni concentrations in the metal due to sulfidation of Fe preferred to Ni. Although the compositional difference between both occurrences of djerfisherite (schreibersite micron-spherule-bearing versus perryite-intergrown) is less significant than those of troilite and sphalerite, the perryite-intergrown grains contain slightly higher Cu than the schreibersite spherule-bearing ones (Lin and El Goresy 2002).

The perryite–sulfide intergrowth was found common in EH3s, but significantly underdeveloped in EL3s. Metallic Fe–Ni nodules in the Almahata Sitta EL3 are usually free of perryite–sulfide intergrowth (Fig. 5d). This difference is consistent with the lower bulk abundance of sulfur (i.e., sulfides) in EL3s than EH3s (Weisberg and Kimura 2012).

3.3 Sulfidation of silicates

In contrast to the gas–solid condensation, another scenario, e.g., sulfidation of silicates, was also proposed to produce oldhamite from diopside and niningerite from Mg-rich olivine and enstatite (Rubin 1983; Fleet and MacRae 1987; Lehner et al. 2013), or destabilization of the gaseous S_2, SiO and Na components dissolved in chondrule melt (Piani et al. 2016). The evidence for sulfidation of silicates includes coexistence of niningerite with corroded silicate clasts (Lehner et al. 2013) and experimental study (Fleet and MacRae 1987). It was suggested that silicate phases may have been sulfurized in an O-poor and S-rich environment, and metal–sulfide nodules in EH3s could have originated and expelled out from the silicate chondrules (Jacquet et al. 2015, 2018). Although sulfides in silicate chondrules could form via sulfidation of silicates and/or crystallization from S-bearing melts, the majority of sulfides, especially metal–sulfide assemblages and the coarse-grained fragments in matrix, are inconsistent with such scenarios, according to the following observations: (1) oldhamite grains with various occurrences have high and similar REE patterns (El Goresy et al. 1988). As depicted above, the REE patterns of oldhamite are consistent with condensation of REE from the nebula under reducing conditions. (2) The REE and other refractory element abundances and patterns are inconsistent with the partitioning coefficients with silicate melt (Ingrao et al. 2019). (3) The normal zoning of niningerite indicates condensation with temperature decreasing, against a solid–gas/melt reaction. (4) The identical features of the schreibersite micron-spherules in oldhamite, niningerite and other sulfides, a robust line evidence for gas–solid condensation as discussed above. (5) The reported evidence for sulfidation of silicates was mainly confined to silicate chondrules, but the majority of sulfides in opaque mineral assemblages and the large sulfide fragments show no reaction textures coexisting with relict silicates.

3.4 Precursor materials of enstatite chondrites

An issue about the precursors of enstatite chondrites was whether they were inherited from presolar dust grains, condensed in situ under reducing conditions, or reduced from FeO-bearing silicates. The presolar grains in primitive chondrites are predominant of submicron- to micron-sized dust grains. Only a few grains of several tens microns were reported so far (Gyngard et al. 2009). Hence, the coarse-grained and euhedral crystals in the primitive chondrites were condensed from the solar nebular gas and/or crystallized from melt droplets. Different from the gas–solid condensation under highly reducing conditions, another scenario proposed that the precursors of enstatite chondrites were ordinary ferromagnesian silicates. The unique sulfides of lithophile elements, such as oldhamite and niningerite, were produced by sulfidation reactions of the silicate precursors under highly reducing conditions (Lehner et al. 2013; Jacquet et al. 2015). However, this scenario is conflict with most petrological observations and mineral chemistry discussed above. The presence of dustlike FeO-bearing silicate clasts in E3 chondrites suggests that they were exotic with FeO reduced to submicron-to-micron-sized metallic Fe particles. This is a convincing line of evidence for the indigenous origin of the predominant FeO-poor enstatite, whereas exotic origin of the dustlike FeO-bearing silicate clasts. The FeO-free pyroxene in enstatite chondrites likely condensed in situ under highly reducing conditions, instead of being reduced from preexisting FeO-bearing silicates.

3.5 Heating events

3.5.1 Chondrules

Similar to other chemical groups of chondrites, silicate chondrules in enstatite chondrites were formed by heating events in the nebular regions but under highly reducing environments followed by fast cooling of the molten droplets. The presence of sulfides in some chondrules and their igneous textures suggest that the melting took place after condensation of troilite and other sulfides. Nine chondrules from the Sahara 97096 EH3 were dated with high-precision Cr isotopes (Zhu et al. 2020). The enstatite chondrite-like chondrules plot on a fossil isochron, resulting in 1.6± 0.7 Ma after Ca- and Al-rich inclusions (Zhu et al. 2020). In addition, Al-rich chondrules from enstatite chondrites have the initial $^{26}Al/^{27}Al$ ratio of $(6.8 \geq 2.4) \times 10^{-6}$ similar to those observed in chondrules from carbonaceous chondrites and unequilibrated ordinary chondrites (Guan et al. 2006), consistent with their similar formation time.

3.5.2 Schreibersite micron-spherules

As discussed above, the wide distribution of micron-spherules of schreibersite in various sulfides suggests a high-temperature heating event in the solar nebula, which melted the preexisting schreibersite. This high-temperature event took place very early, predating the condensation of oldhamite and all other sulfides. Furthermore, the heating event likely happened in the same regions where the constituent minerals of enstatite chondrites, including schreibersite and various sulfides, were condensing from the nebula under a reducing condition. This is different from the silicate chondrule-forming events, which postdated most of silicates and probably troilite and the heating site could be different from the condensation regions (Hewins 1997; Lauretta et al. 2006).

3.5.3 Opaque nodules

Evidence for melting: In both EH3s and EL3s, it is common that the metal–sulfide assemblages occur as round shapes, generally referred to as opaque nodules. The round or oval shapes of opaque assemblages imply that they were once molten as silicate chondrules, probably by the same heating events in the protoplanetary disk. In addition, there are also kamacite–silicate intergrowths in EH3s and EL3s, which formed probably via pre-accretionary melting based on the highly siderophile and other trace element abundance patterns of the metal grains (Horstmann et al. 2014). If the opaque nodules were once molten, the heating event likely predated the sulfidation of metal, since the intergrowth of sulfides and perryite usually occurs along the peripheries of the nodules.

Evidence for non-melting: Regardless of the round or oval shapes, the opaque nodules may not be melted but accretion of condensates. As discussed above, the schreibersite micron-spherule-bearing sulfides are gas–solid condensates. These schreibersite micron-spherule-bearing sulfides are commonly present in the centers of metal–sulfide nodules (Fig. 4d) (e.g., Figure 1a by Lin and El Goresy (2002)), showing identical morphologies and mineral chemistry of those fragments in matrix. If the metal–sulfide nodules were molten droplets, troilite (and also other sulfides) would have been melted together with metal, producing en eutectic texture between metal and troilite and merging schreibersite micron-spherules together. These observations are against melting of the metal–sulfide nodules. Furthermore, the metal–perryite–sulfide intergrowths occur mainly along the peripheries of the nodules, suggestive of the sulfidation postdating the nodules. No melting of the nodules took place after the sulfidation, otherwise the two textural features of troilite (the irregular grains intergrown with perryite, the coarse and euhedral grains entrapping schreibersite micron-spherules) could not have been preserved in the same nodules (Fig. 4d) (e.g., Figure 1a,b by Lin and El Goresy (2002)). In addition, as discussed above, the sulfidation took place after the formation of nodules. In contrast, sulfides in silicate chondrules often show igneous textures (Piani et al. 2016), indicating that the chondrule-heating events postdated formation of troilite and other sulfides. These observations are inconsistent with the possible simultaneous melting of the opaque nodules and silicate chondrules in enstatite chondrites by the same heating events.

In the EL3 Almahata Sitta, many metal nodules exhibit zoning textures, with one and multilayers of abundant fine-grained enstatite and sinoite crystals between metallic Fe–Ni. In addition, under high-contrast BSE images, the metallic Fe–Ni appears as assemblages of individual euhedral grains (El Goresy et al. 2017). Prisms of enstatite are mainly intergrown with metal along the margins or the rims of the nodules. The zoning texture was also reported in opaque nodules in many EH3s, including Qingzhen (Lin and El Goresy 2002), Y-691, Sahara 97159 and the paired ones (Weisberg and Kimura 2012; Jacquet et al. 2018), and Kaidun (EH3-4) (Ivanov et al. 1996). Lehner et al. (2017) reported porous and S-bearing silica in metal–sulfide nodules from two EH3 chondrites, which also show accretionary textures with silicate-rich layers.

Various silicate inclusions in metal nodules from Kaidun (EH3-4) appear to be related to condensation of material onto the surfaces of metal grains (Ivanov et al. 1996). The nodules appear to have formed by aggregation of separate grains (globules) of metal, with conservation of condensates on the grain surfaces as inclusions. The inclusions probably condensed in a wide temperature range from 1400 to 600 K (Ivanov et al. 1996). The aggregation of metal grains and formation of the nodules probably occurred simultaneously with condensation (Ivanov et al. 1996). All sinoites in the EL3 Almahata Sitta were found in metallic Fe–Ni, probably condensed before or together with metal. Although impact origin of sinoite was proposed (Rubin 1997), these enstatite chondrites are not primitive type 3 but impact melts. The very high abundance of sinoite in metal, up to 22 vol% in the EL3 Almahata Sitta (El Goresy et al. 2017), argues against exsolution of sinoite from the metal.

It was also noticed that chromium sulfides, including daubréelite, aqueous $FeCrS_4$, minerals A and B, and caswellsilverite, usually occur in the margins and/or the rims of the metal nodules. Lawrencite ($FeCl_2$) was also reported as rims of assemblages in Indarch (Keil 1968) but more common as inclusions in metallic Fe–Ni in unequilibrated enstatite chondrites; probably, it can be preserved better as inclusions in metal since this phase is extremely sensitive to humidity. Two types of graphite were found in the Almahata Sitta EL3 (El Goresy et al.

2017), as sphere-shaped assemblages of dendritic crystals enclosed in metallic Fe–Ni in MS-17 and as books in silicate matrix in MS-177.

In summary, the silicate chondrules in enstatite chondrites are similar to those in carbonaceous and ordinary chondrites, produced by transient heating events in the solar nebula. Although opaque nodules appear round or oval in shapes, implying once melted as silicate chondrules, detailed petrological observations favor aggregation of condensates.

3.5.4 Material transportation

Enstatite chondrites condensed and accreted under extremely reducing conditions in the protoplanetary disk, probably closest to the proto-Sun (Wasson 1988; Rubin 2011). There are also components in enstatite chondrites that formed under higher oxygen fugacities and other conditions, and hence they are probably exotic. These candidate exotic components were transported from other regions before or during accretion of enstatite chondrites. Another scenario is that the FeO-rich components are relicts after the local conditions evolved into highly reducing conditions.

3.5.5 Ca-, Al-rich inclusions

Ca-, Al-rich inclusions (CAIs) were reported as minor components in enstatite chondrite (Bischoff et al. 1985; Fagan et al. 2000; Guan et al. 2000b; Lin et al. 2003), and they share the same initial $^{26}Al/^{27}Al$ ratio of $\sim 5 \times 10^{-5}$ as those typical of carbonaceous chondrites. In addition, the oxygen isotopes of CAIs from enstatite chondrites plot on the same line with slope of ~ 1.0 in the three-isotope plot, identical to the isotopic compositions of unaltered minerals in CAIs from carbonaceous chondrites (Guan et al. 2000a; Fagan et al. 2001; Lin et al. 2003).

The EH3 Sahara 97159 contains unusually high abundance of CAIs, with 68 found in two polished sections, or 22 per cm^2 (0.06 vol%). All of the inclusions are intensely altered, and the alteration assemblages with the presence of FeO-poor spinel suggest that the alteration took place under reducing and SiO_2-rich conditions, consistent with enstatite chondrite-accreting environments. The pre-altered mineral assemblages are type A-like or spinel–pyroxene-rich ones similar to the predominant types in carbonaceous chondrites, indicative of their same origins and delivered from the same reservoirs (Lin et al. 2003).

3.5.6 Relict silicates and chondrules

Minor dusty FeO-bearing silicate clasts were found in enstatite chondrites, which contain abundant tiny Ni-poor and Cr-rich metallic Fe (Rambaldi et al. 1984; Weisberg et al. 1994; Lin et al. 2002b). These clasts were proposed to originate in the same general nebular neighborhood of enstatite chondrites and were subsequently transported into the reducing environments (Rambaldi et al. 1984). Weisberg et al (2011) analyzed oxygen isotopes of the FeO-bearing silicate clasts and found the $\Delta^{17}O$ values of some olivine and pyroxene from E3s plotting outside of the enstatite chondrite range, with one close to R group and several to carbonaceous chondrites. Jacquet et al. (2018) also summarized $\Delta^{17}O$ values of several ten chondrules in enstatite chondrites, overlapping with those of LL3. On the other hand, majority of the FeO-rich pyroxenes have the same oxygen isotopes of the enstatite, and they were proposed to have formed at different times under different redox conditions but from the same oxygen reservoir (Weisberg et al. 2011). Alternatively, the similar $\Delta^{17}O$ values of these components within the range of enstatite chondrites could also be explained by isotope exchange with the local oxygen reservoir of enstatite chondrites, as indicated by the reduction textures of the dusty FeO-bearing silicate clasts.

Zhu et al (2020) analyzed Cr isotopes of chondrules from the Sahara 97096 EH3 and found that two out of nine chondrules have definitely ^{54}Cr-anomaly (ε up to 1.01 ± 0.11) within the range of carbonaceous group. The discovery of carbonaceous group chondrules in enstatite chondrites suggests early transportation of materials from the outer solar system to the enstatite chondrite-accreting regions in the inner solar system. This scenario is supported by numerical simulations of chondrule transportation in the protoplanetary disk (Goldberg et al. 2015).

4 Processes in the parent bodies

4.1 Thermal metamorphism

The FeS content of both niningerite and alabandite in contact with troilite positively correlates with temperature. Two types of normal zoning and one type of reverse zoning of niningerite were reported in Qingzhen (Lin and El Goresy 2002). The normal zoning of niningerite, with the FeS content decreasing from 17.5 mol% in the centers to 15.4 mol% at the rims in contact with silicate and/or oldhamite, probably indicates condensation as temperature decreased, whereas the other normal zoning of niningerite, with the FeS content decreasing from 17.7 mol% to 15.2 mol% toward troilite, suggests equilibrium diffusion of FeS at lower temperature probably in the parent body. This is consistent with exsolution of troilite in niningerite in Qingzhen (Lin and El Goresy 2002). The same normal zoning and exsolution of troilite were also found in alabandite in the EL3 MAC 88136, due to a slow cooling in the parent body. As shown in Fig. 2, the FeS contents of niningerite in EHs and alabandite in ELs are generally correlated with the petrographic types. However, a few of EH and EL chondrites deviates from

this trend, e.g., the EH5 St. Marks and QUE 93372 overlapping the range of EH3s, and Jajh deh Kot Lalu (EL6) within the range of EL3. In addition, the (Mg, Mn, Fe)S solid solution in the EH impact melt rocks are usually FeS-rich, named as keilite. These observations can be explained by re-accretion of breakup original parent bodies; however, additional evidence is required to make up a detailed model. Alternatively, Weyrauch et al. (2018) divided EH and EL into EHa, EHb, and ELa, ELb, respectively, based mainly on Fe contents in (Fe, Mg, Mn)S and Cr contents in troilite. They proposed different parent bodies for these subgroups of enstatite chondrites. However, as discussed above, the systematic variation in the MnS content of sulfides, especially the presence of niningerite in EH and alabandite in EL, was established during nebular processes under different conditions. In contrast, the Fe contents of (Fe, Mg, Mn)S and Cr contents of troilite could be modified by thermal metamorphism in the parent bodies. Hence, it is not necessary to further divide EH and EL groups based on these thermal metamorphism-related parameters.

The FeS content of sphalerite in contact with troilite is also dependent on temperature and/or pressure (Balabin and Urusov 1995). Sphalerite shows variation in the FeS contents within and/or among grains with a relatively constant MnS content (Fig. 3). The normal zoning profiles of sphalerite, with the FeS contents decreasing from 50.8 mol% in the cores to 46.0 mol% in contact with troilite, were reported in Qingzhen (Lin and El Goresy 2002). The FeS content of ~ 46 mol% of sphalerite in contact with troilite suggests a final equilibrium temperature of ~ 500 K according to the thermometer of sphalerite (Balabin and Urusov 1995), assuming a shallow buried depth.

Troilite contains minor Cr and often shows exsolution of daubréelite, which is another indicator of thermal history. In Qingzhen, it is noticed that troilite in contact with Cr sulfides always shows exsolution of tiny daubréelite (Lin and El Goresy 2002). This texture can be explained by two stages of CrS diffusion, first from the adjacent Cr sulfides into troilite during heating and followed by exsolution of tiny daubréelite from the Cr-bearing troilite during cooling. This observation suggests that the Cr content and exsolution of daubréelite from troilite are very sensitive to the thermal history. Weyrauch et al. (2018) divided EH and EL into high and low subgroups based on the Cr contents of troilite and the FeS contents of (Mg, Mn, Fe)S solid solution.

The Si contents of metallic Fe–Ni in E3s can be referred to as indicator of oxygen fugacity of the nebula, and their variations may reflect heterogeneous redox conditions within EH and EL regions. However, the Si contents of equilibrated enstatite chondrites could be affected by thermal metamorphism, as indicated in Fig. 1. The Si contents of metal intend to increase with thermal metamorphism (Weyrauch et al. 2018).

4.2 Shock metamorphism

Enstatite chondrites commonly experienced shock metamorphism, with many meteorites classified as impact melt rocks. Some enstatite meteorites, previously classified as aubrites, were re-designated as EH impact melts, based on their undifferentiated modal abundances, presence of niningerite, graphite and high Si content of metal (Udry et al. 2019). Rubin (2015) summarized the shock features of enstatite chondrites and proposed a classification scheme of shock metamorphism. Both EHs and ELs show correlations between petrologic type and the degree of shock, which suggest that collisional heating is mainly attributed to the thermal metamorphism of enstatite chondrites. This also explains the relatively young Ar–Ar ages of enstatite chondrites. Furthermore, most Fe-rich niningerites (i.e., keilite) are present in EH melt rocks, except for LEW 88180 classified as EH5-6 (Zhang et al. 1995) but re-designated as IMB (Keil 2007). The presence of keilite in EH impact melt consists of quenching of shock-induced melts. On the other hand, no keilite was reported in EL impact melt, except for EET 90102 (EL6) (Fogel 1997). In addition, keilite was found in Khor Temiki #2 vitrophyre in the aubrite host (Fogel 2005). This observation supports the distinct post-shock thermal histories of EH and EL parent bodies.

Oldhamite and other sulfides can crystallize from enstatite chondrite impact melts, based on the experiments with Indarch as starting material (McCoy et al. 1997a, b; McCoy et al. 1999). The shock-induced silicate melts can incorporate significant S, and the compositions of the melts are related to the temperature. Metal–sulfide melts completely at 1000 °C, whereas silicates start to melt at 1000 °C and complete at 1500 °C. The post-shock temperature is based on shock pressure and the porosity of the targets (Moreau et al. 2019), the post-shock temperatures increasing from ~ 540 K at 30 GPa to ~ 1300 K at 70 GPa, and the post-shock temperature increases by ~ 800 K and melt fraction by ~ 0.12 with the porosity increasing up to 15%.

4.3 Qingzhen reaction

Djerfisherite is commonly present in enstatite chondrites and usually occurs as large fragments in matrix. It shows a breakup texture, partially replaced with fine-grained troilite and trace sphalerite (Fig. 4a), which was referred to as "Qingzhen Reaction" by El Goresy (1995). The fine-grained sphalerite in the breakdown products of djerfisherite has the lowest FeS content of ~ 42 mol%, indicative of low temperature of < 450 K (Lin and El Goresy 2002).

Isotopic analysis of the breakup products of djerfisherite in Qingzhen shows that the I-Xe chronometer is decoupled from, and more stable than, both Ar–Ar and Rb–Sr chronometers, which were reset in the 1.4–2.8 Ga period (Ash et al. 1997).

Hopp et al. (2014) conducted Ar–Ar dating of enstatite chondrites and found different Ar–Ar age distribution between EHs and ELs. The Ar–Ar ages of ELs are in a narrow range from 4.50–4.44 Ga, whereas EHs are more variable from 4.55 to 2.2 Ga. The very young ages show clear evidence for impact-induced partial resetting at ~ 2.2 Ga, consistent with the I-Xe results of the breakdown products of djerfisherite. The isotope chronology of EHs and ELs also supports the different metamorphism histories of their parent bodies.

5 Implications to the Earth building components

5.1 Isotopic compositions

The isotopic anomalies, e.g., $\Delta^{17}O$, $\varepsilon^{50}Ti$ and $\varepsilon^{54}Cr$, were little affected by the solar nebular processes, but preserved the information of the reservoirs. Accordingly, the available materials of the solar system have been classified into the carbonaceous group (representative of outer solar system) and the non-carbonaceous group (representative of inner solar system) (Warren 2011). The Earth, the Moon and enstatite meteorites belong to the non-carbonaceous group and have identical isotopic compositions. These discoveries supply with strong evidence for the genetic relationship of enstatite meteorites and the Earth, which were confirmed by analyses of many other elements.

Lithophile elements: The Ca isotopes imply multiple supernova sources for the neutron-rich isotopes in the solar system, with $\varepsilon^{48/44}Ca$ and $\delta^{44/40}Ca$ varying up to ~ 1‰ in chondrites, whereas enstatite chondrites and the Earth have identical Ca isotopic compositions (Huang and Jacobsen 2017). Although there is an average small deficit of ~ 10 ppm in ^{142}Nd of enstatite chondrites relative to modern terrestrial samples, the closest to the Earth value, the $\mu^{142}Nd$ average value of EL3s is -0.8± 7.0(2SD) (Boyet et al. 2018). In addition, the $\varepsilon^{96}Zr$ values of enstatite chondrites are the same of the bulk silicate Earth (BSE) (Mezger et al. 2020).

Although Si isotopes of enstatite chondrites appear lighter by ~ 0.30‰ $\delta^{30}Si$ in comparison with the BSE, which was used to argue against any major contribution of enstatite chondrite-like planetary materials in Earth accretion (Fitoussi and Bourdon 2012), this discrepancy could be due to fractionation of Si between silicates and Si-bearing metal during condensation. Sikdar et al. (2020) analyzed metal and silicate separates from EH3 and reported significantly lighter Si isotopes in enstatite chondrite metals ($\delta^{30}Si \geq -6.94 \pm 0.09$‰, Mg/Si = ~ 0.001), whereas its silicates are heavier (av. $\delta^{30}Si = -0.33 \pm 0.11$‰, Mg/Si = ~ 1.01) and closer to BSE ($\delta^{30}Si = -0.29 \pm 0.08$‰). First-principles calculations of equilibrium isotopic fractionation of Si during condensation of the solar nebula under highly reducing conditions confirmed that the silicates are ^{30}Si-enriched in comparison with Si-bearing metallic Fe–Ni (Javoy et al. 2012).

Refractory siderophile elements: highly siderophile elements in the terrestrial mantle are mainly attributed to the late veneer, because the original inventory has been partitioned into the core during the metal–silicate segregation. Hence, the isotopes of highly siderophile elements of the Earth's mantle trace mainly the features of the late veneer. The $\varepsilon^{100}Ru$ values of enstatite chondrites are the closest to the Earth value (Fischer-Gödde and Kleine 2017), suggesting that not carbonaceous chondrites but enstatite chondrites may be the primary late veneer. The $\mu^{92}Mo$ and $\varepsilon^{100}Mo$ values (*s*-process component) show the same trend as Ru isotopes, with enstatite chondrites closest to the Earth's mantle (Render et al. 2017; Mezger et al. 2020).

Moderate volatile elements: Zhao et al. (2020) analyzed K isotopes of 8 enstatite chondrites and reported the average δ^{41} K of 0.47±0.57‰, indistinguishable from the BSE value (0.48 ± 0.03‰). $\delta^{66/64}Zn$ of enstatite chondrites (0.2–0.4‰) is similar to the Earth (0.3‰), and the $\delta^{122/118}Sn$ value is only slightly lighter (0.18 ± 0.21‰) than the Earth (0.49 ± 0.11‰). The isotopically heavy Sn of the silicate Earth may be due to loss of light Sn, via partition into the metallic core or a sulfide matter, or by evaporative loss from Earth. This isotopically light Sn loss is consistent with the correlation between the contents and isotopic compositions (Creech and Moynier 2019).

5.2 Bulk chemistry

The isotopic similarity of enstatite chondrites with the Earth suggests that they could be the major building blocks of the latter. The most significant chemical difference between enstatite chondrites and BSE is the higher SiO_2 abundance of enstatite chondrites. However, this chemical difference can be explained by differentiation processes in the early Earth (Javoy 1995; Javoy et al. 2010). During core formation, the exchange budget equation $SiO_2 + 2Fe = Si + 2FeO$ under high pressure and temperature can deduce the compositions of BSE, the lower mantle and the core from enstatite chondrites. The building blocks of the Earth were chemically and isotopically similar, but not identical to, enstatite chondrites.

The origins of water and volatile components of the Earth are another long-standing issue. A model is that the building blocks of the Earth are very dry and the majority of water was delivered by the late veneer of carbonaceous chondrites. Maruyama et al. (2017) proposed

formation of the Earth as two steps. At 4.56 Ga, the Earth was born from enstatite chondrite-like dry materials without atmosphere and ocean components, and peaked at 4.37–4.2 Ga the subsequent secondary accretion of bio-elements, H, C, O and N probably from carbonaceous chondrites. This model was referred to as ABEL (the advent of bio-elements model). However, the isotopic compositions of highly siderophile elements favor for addition of the s-process deficit carbonaceous chondrites. On the other hand, the primitive enstatite chondrites may not mean dry or volatile-poor, because of the presence of the aqueous Cr sulfides (minerals A and B, aqueous Fe–Cr sulfide), sinoite and graphite as depicted above. These aqueous Cr sulfides are not terrestrial weathering origins, since the Qingzhen and several other enstatite meteorites are witnessed falls. In fact, the bulk compositions of enstatite chondrites (especially EH3s) do not show significant depletion in moderate volatile elements. Furthermore, the analysis of water contents and H isotopes of enstatite chondrites reveals that the water contents ranging from 0.08 to 0.54 wt% (negatively correlated with type) with bulk δ D of -100 ~ − 150‰, and enstatite chondrites attributed at least three times the mass of water in the ocean (Piani et al. 2020).

Of the meteorite collection, enstatite chondrites show the most similar isotopic compositions of the Earth, suggestive of important contribution to the building materials of the latter. However, there are large differences in bulk compositions between the Earth's mantle and enstatite chondrites (e.g., higher FeO content of the former, whereas more SiO2 of the latter), which are required to be addressed in detail. Nevertheless, the highly reduced properties, high abundance of graphite, and the presence of N-bearing phases and aqueous Cr sulfides of enstatite chondrites could have critical constraints on the early evolution of the Earth and the compositions of terrestrial mantle and core.

6 Issues remained

6.1 Relative abundances of presolar grains

Presence of Si_3N_4: SiC is not expected to condense under the conditions of carbonaceous chondrites or ordinary chondrites; hence, its presolar origins are understandable. In contrast, SiC can condense under highly reducing conditions (Larimer and Bartholomay 1979), but all SiC grains from the primitive enstatite chondrites are presolar origins. This discovery indicates that in fact no SiC condensed under the highly reducing conditions in the solar nebula. On the other hand, few AGB grains of Si_3N_4 have been found in meteorites (Zinner et al. 2007), although Si_3N_4 grains were detected in the circumstellar shells of a number of extreme carbon stars (Clément et al. 2005) and the predominant Si_3N_4 grains in enstatite chondrites are solar origin (Lin et al. 2002a). A part of Si_3N_4 grains were likely exsolution from metallic Fe–Ni, usually with a needle-like shape (Alexander et al. 1994). Other Si_3N_4 grains found in metal, schreibersite, sulfides and silicates probably condensed in the solar nebula with δ^{15} N of -60 ± 1‰ (Leitner et al. 2018). All of the presolar Si_3N_4 grains are supernova origin (Nittler et al. 1995; Lin et al. 2002a). The relative abundance of X-Si_3N_4 is comparable with that of X-SiC, suggestive of condensation of both phases from the supernovae ejecta. In contrast, SiC but no Si_3N_4 condensed from AGB ejecta, whereas both were reverse in the reduced solar nebula.

Rareness of presolar O-rich grains: The matrix-normalized abundances of presolar SiC and diamond in Qingzhen are comparable to those in Murchison and other primitive chondrites. However, the presolar O-rich grains are extremely depleted in Qingzhen (Lin et al. 2002a). This discrepancy is remarkable, regarding that the relative abundances of various types of presolar SiC and Si_3N_4 grains are similar between enstatite chondrites and carbonaceous chondrites (Lin et al. 2002a). A scenario is that the presolar O-rich grains have been largely destroyed under the highly reducing environments. This scenario may be attributed to the absence of presolar silicates in enstatite chondrites. However, corundum and spinel are very stable and resistant to strong acid, and they were separated via being concentrated in the acid residue of chondrites.

6.2 Coexistence of high-T condensates and low-T preservation of presolar grains

The submicron-sized presolar grains are very sensitive to temperature. The abundance of presolar grains in E3 chondrites is comparable to those of ordinary chondrites and carbonaceous chondrites. This discovery supplies with robust evidence that the temperature at chondrite-accreting regions was low and there was no significant increase in temperature from carbonaceous chondrites in the outer solar system to enstatite chondrites in the inner solar system. On the other hand, the majority of the constituent minerals in enstatite chondrites condensed at high temperature under highly reducing conditions. The coexistence of high-T condensates and low-T preservation of presolar grains suggests that both components formed and preserved in separated areas and finally transported into the enstatite chondrite-accreting regions. However, it is unknown whether the presolar grains were added from the low-T zones of the outer solar system and/or from the periphery of the protoplanetary disk to the midplane, or the main constituents condensed at high-T zones of the protoplanetary disk and transported outward into enstatite chondrite-accreting regions.

The systematically different mineral chemistry between EHs and ELs favors local condensation and consequent in situ accretion without significant transportation. This scenario is supported by the relatively constant mineral chemistry within the same chondrites, e.g., the Mn contents of sulfides, which indicate similar forming conditions of the minerals in the same chondrites but show spatial variation. Graphite from Almahata Sitta MS-17 and MS-177 EL3 has distinct morphologies and C isotopic compositions (MS-177: books in silicate matrix with $\delta^{13}C = -18$ to -2‰; MS-17: feathery spherules in metal with $\delta^{13}C = -26$ to -6‰) (El Goresy et al. 2017). Not only the differences between EH and EL regions, but also within ELs and EHs, the chemical and isotopic variations have been well preserved during accreting process. Preservation of the delicate differences established during condensation supplies with convincing evidence for local accretion of enstatite chondrites. This discovery favors a scenario that the presolar grains were added from low-T zones.

6.3 Origins of the highly reducing conditions

The solar nebula has a bulk composition of CI chondrites with the C/O ratio of ~ 0.54. The enstatite chondrite-forming regions were highly reducing with C/O ratios > 0.8, different from the canonical value of the solar nebula. Before condensation from high temperature, the enstatite chondrite-forming regions should have been evolved into highly reduced conditions from the homogeneous solar nebula with a CI composition. As discussed above, repeating evaporation and condensation of water ice and organic matter cross the snow line along the protoplanetary disk could produce an increasing C/O ratio toward the Sun. Isotopic compositions of N and C of insoluble organic matter (IOM) from Sahara 97096 (EH3) are within the range of values observed for carbonaceous chondrites, suggestive of a common component widespread in the solar nebula (Piani et al. 2012).

Furthermore, enstatite chondrite-forming regions could be rather heterogeneous with a large gradient in oxygen fugacity from EH to EL regions, as indicated by the Si contents of metal, the MnS contents of sulfides and C isotopes of graphite. However, few records of the evolutional processes have been found.

Pignatale et al. (2016) computed a 2D condensation model for the inner solar nebula. They found that an enstatite-rich environment could be achieved via vertical settling and radial migration of dust in the protoplanetary disk, and enstatite chondrites could form in the inner surface layer of the disk within 0.4 AU.

Acknowledgements
The author is grateful to Prof. Ahmed El Goresy for his supervision when the author conducted his PhD thesis research in the Max Planck Institute für Kernphysik, Heidelberg, more than 30 years ago. The manuscript has been significantly improved by the constructive reviews by Dr. M. Kimura and A. E. Rubin and the guest editor T. Sharp. This work was supported by the Strategic Priority Research Program on Space Science, Chinese Academy of Sciences (XDA15020300), the Key Research Program of Frontier Sciences, CAS (QYZDJ-SSW-DQC001), and the Natural Science Foundation of China (41673069).

Author contributions
YL contributed to the review and writing of the paper. The author read and approved the final manuscript.

Funding
Funding for this work was provided by the Strategic Priority Research Program on Space Science, Chinese Academy of Sciences (XDA15020300), the Key Research Program of Frontier Sciences, CAS (QYZDJ-SSW-DQC001), and the Natural Science Foundation of China (41673069).

Availability of data and materials
Please contact the author for data requests.

Declarations

Competing interests
The author declares that he has no competing interests.

Received: 8 November 2021 Accepted: 6 May 2022
Published online: 20 May 2022

References

Alexander CMOD, Swan P, Prombo CA (1994) Occurrence and implications of silicon nitride in enstatite chondrites. Meteoritics 29:79–84
Ash R D, Gilmour J D, Whitby J, Prinz M and Turner G (1997) I-Xe dating of chondrules from the Qingzhen unequilibrated enstatite chondrite (abstract). Lunar and Planetary Science Conference XXVIII:61–62
Balabin AI, Urusov VS (1995) Recalibration of the sphalerite cosmobarometer: experimental and theoretical treatment. Geochim Cosmochim Acta 59:1401–1410
Bischoff A, Keil K, Stoeffler D (1985) Perovskite-hibonite-spinel-bearing inclusions and Al-rich chondrules and fragments in enstatite chondrites. Chem Erde 44:97–106
Boyet M, Bouvier A, Frossard P, Hammouda T, Garcon M, Gannoun A (2018) Enstatite chondrites EL3 as building blocks for the Earth: The debate over the ^{146}Sm–^{142}Nd systematics. Earth Planet Sci Lett 488:68–78
Boyet M, Gannoun A (2013) Nucleosynthetic Nd isotope anomalies in primitive enstatite chondrites. Geochim Cosmochim Acta 121:652–666
Clément D, Mutschke H, Klein R, J ger C., Dorschner J., Sturm E. and Henning T. (2005) Detection of silicon nitride particles in extreme carbon stars. Astrophys J 621:985
Creech J, Moynier F (2019) Tin and zinc stable isotope characterisation of chondrites and implications for early solar system evolution. Chem Geol 511:81–90
Crozaz G, Floss C, Wadhwa M (2003) Chemical alteration and REE mobilization in meteorites from hot and cold deserts. Geochim Cosmochim Acta 67:4727–4741
Crozaz G, Lundberg LL (1995) The origin of oldhamite in unequilibrated enstatite chondrites. Geochim Cosmochim Acta 59:3817–3831
Davidson J, Schrader DL, Alexander CMOD, Lauretta DS, Busemann H, Franchi IA, Greenwood RC, Connolly HC, Domanik KJ, Verchovsky A (2014) Petrography, stable isotope compositions, microRaman spectroscopy, and presolar components of roberts massif 04133: A reduced CV3 carbonaceous chondrite. Meteorit Planet Sci 49:2133–2151
Fagan TJ, Krot AN, Keil K (2000) Calcium-aluminum-rich inclusions in enstatite chondrites (I): Mineralogy and textures. Meteorit Planet Sci 35:771–781

Fagan TJ, McKeegan KD, Krot AN, Keil K (2001) Calcium-aluminum-rich inclusions in enstatite chondrites (II): Oxygen isotopes. Meteorit Planet Sci 36:223–230
Fegley B Jr (1982) Chemical fractionations in enstatite chondrites. Meteoritics 17:210–212
Fischer-Gödde M, Kleine T (2017) Ruthenium isotopic evidence for an inner solar system origin of the late veneer. Nature 541:525
Fitoussi C, Bourdon B (2012) Silicon isotope evidence against an enstatite chondrite Earth. Science 335:1477–1480
Fleet ME, MacRae ND (1987) Sulfidation of Mg-rich olivine and the stability of niningerite in enstatite chondrites. Geochim Cosmochim Acta 51:1511–1521
Fogel RA (1997) On the significance of diopside and oldhamite in enstatite chondrites and aubrites. Meteorit Planet Sci 32:577–591
Fogel RA (2005) Aubrite basalt vitrophyres: the missing basaltic component and high-sulfur silicate melts. Geochim Cosmochim Acta 69:1633–1648
Goldberg AZ, Owen JE, Jacquet E (2015) Chondrule transport in protoplanetary discs. Mon Not R Astron Soc 452:4054–4069
El Goresy A (1995) The Qingzhen reaction: fingerprints of the EH planet? Meteorit Planet Sci 20:639
El Goresy A, Lin Y, Miyahara M, Gannoun A, Boyet M, Ohtani E, Gillet P, Trieloff M, Simionovici A, Feng L, Lemelle L (2017) Origin of EL3 chondrites: evidence for variable C/O ratios during their course of formation-A state of the art scrutiny. Meteorit Planet Sci 52:1–26
El Goresy A, Yabuki H, Ehlers K, Woolum D, Pernicka E (1988) Qingzhen and Yamato-691: a tentative alphabet for the EH chondrites. Proc NIPR Symp Antarct Meteorites 1:65–101
Guan Y, Huss GR, Leshin LA, MacPherson GJ, McKeegan KD (2006) Oxygen isotope and ^{26}Al-^{26}Mg systematics of aluminum-rich chondrules from unequilibrated enstatite chondrites. Meteorit Planet Sci 41:33–47
Guan Y, Huss GR, MacPherson GJ, Wasserburg GJ (2000b) Calcium-aluminum-rich inclusions from enstatite chondrites: indigenous or foreign? Science 289:1330–1333
Guan Y, McKeegan KD, MacPherson GJ (2000a) Oxygen isotopes in calcium-aluminum-rich inclusions from enstatite chondrites: new evidence for a single CAI source in the solar nebula. Earth Planet Sci Lett 181:271–277
Gyngard F, Amari S, Zinner E, Ott U (2009) Interstellar exposure ages of large presolar SiC grains from the Murchison meteorite. Astrophys J 694(1):359
Hewins RH (1997) Chondrules. Annu Rev Earth Planet Sci 25:61–83
Hopp J, Trieloff M, Ott U, Korochantseva EV, Buykin AI (2014) Ar^{39}-Ar^{40} chronology of the enstatite chondrite parent bodies. Meteorit Planet Sci 49:358–372
Horstmann M, Humayun M, Bischoff A (2014) Clues to the origin of metal in Almahata Sitta EL and EH chondrites and implications for primitive E chondrite thermal histories. Geochim Cosmochim Acta 140:720–744
Hsu W (1998) Mineral chemistry and the origin of enstatite in unequilibrated enstatite chondrites. Geochim Cosmochim Acta 62:1993–2004
Huang S, Jacobsen SB (2017) Calcium isotopic compositions of chondrites. Geochim Cosmochim Acta 201:364–376
Huss G, Lewis RS (1995) Presolar diamond, SiC, and graphite in primitive chondrites: abundances as a function of meteorite class and petrologic type. Geochim Cosmochim Acta 59:115–160
Ingrao NJ, Hammouda T, Boyet M, Gaborieau M, Moine BN, Vlastelic I, Bouhifd MA, Devidal JL, Mathon O, Testemale D, Hazemann JL, Proux O (2019) Rare earth element partitioning between sulphides and melt: evidence for Yb^{2+} and Sm^{2+} in EH chondrites. Geochim Cosmochim Acta 265:182–197
Ivanov AV, MacPherson GJ, Zolensky ME, Kononkova NN, Migdisova LF (1996) The Kaidun meteorite: composition and origin of inclusions in the metal of an enstatite chondrite clast. Meteorit Planet Sci 31:621–626
Jacquet E, Alard O, Gounelle M (2015) The formation conditions of enstatite chondrites: insights from trace element geochemistry of olivine-bearing chondrules in Sahara 97096 (EH3). Meteorit Planet Sci 50:1624–1642
Jacquet E, Piani L and Weisberg M K (2018) Chondrules in enstatite chondrites. In: chondrules: records of protoplanetary disk processes: Cambridge University Press https://doi.org/10.1017/9781108284073.007.
Javoy M (1995) The integral enstatite chondrite model of the Earth. Geophys Res Lett 22:2219–2222
Javoy M, Balan E, Méheut M, Blanchard M, Lazzeri M (2012) First-principles investigation of equilibrium isotopic fractionation of O- and Si-isotopes between refractory solids and gases in the solar nebula. Earth Planet Sci Lett 319–320:118–127
Javoy M, Kaminski E, Guyot F, Andrault D, Sanloup C, Moreira M, Labrosse S, Jambon A, Agrinier P, Davaille A, Jaupart C (2010) The chemical composition of the earth: enstatite chondrite models. Earth Planet Sci Lett 293:259–268
Keil K (1968) Mineralogical and chemical relationships among enstatite chondrites. J Geophys Res 73:6945–6976
Keil K (2007) Occurrence and origin of keilite, (Fe>0.5, Mg<0.5)S, in enstatite chondrite impact-melt rocks and impact-melt breccias. Chem Erde 67:37–54
Kimura M, Weisberg MK, Lin Y, Suzuki A, Ohtani E, Okazaki R (2005) Thermal history of the enstatite chondrites from silica polymorphs. Meteorit Planet Sci 40:855–868
Larimer JW, Bartholomay M (1979) The role of carbon and oxygen in cosmic gases: some applications to the chemistry and mineralogy of enstatite chondrites. Geochim Cosmochim Acta 43:1455–1466
Larimer JW, Ganapathy R (1987) The trace element chemistry of CaS in enstatite chondrites and some implications regarding its origin. Earth Planet Sci Lett 84:123–134
Lattimer JM, Grossman L (1978) Chemical condensation sequences in supernova ejecta. Moon Planet 19:169–184
Lauretta DS, Nagahara H, Alexander CMO, d. (2006) Petrology and origin of ferromagnesian silicate chondrules. Meteor Early Solar Sys II:431–459
Lehner SW, Buseck PR, McDonough WF (2010) Origin of kamacite, schreibersite, and perryite in metal-sulfide nodules of the enstatite chondrite Sahara 97072 (EH3). Meteorit Planet Sci 45:289–303
Lehner SW, Nemeth P, Petaev MI, Buseck PR (2017) Porous, S-bearing silica in metal-sulfide nodules and in the interchondrule clastic matrix in two EH3 chondrites. Meteorit Planet Sci 52:2424–2436
Lehner SW, Petaev MI, Zolotov MY, Buseck PR (2013) Formation of niningerite by silicate sulfidation in EH3 enstatite chondrites. Geochim Cosmochim Acta 101:34–56
Leitner J, Vollmer C, Henkel T, Ott U, Hoppe P (2018) An isotopic, elemental and structural study of silicon nitride from enstatite chondrites. Geochim Cosmochim Acta 235:153–172
Lewis RS, Tang M, Wacker JF, Anders E, Steel E (1987) Interstellar diamonds in meteorites. Nature 326:160–162
Lin Y, Amari S, Pravdivtseva O (2002a) Presolar grains from the Qingzhen (EH3) meteorite. Astrophys J 575:257–263
Lin Y, El Goresy A (2002) A comparative study of opaque phases in Qingzhen (EH3) and MAC 88136 (EL3): Representative of EH and EL parent bodies. Meteorit Planet Sci 37:577–599
Lin Y, Guo J, Hu S, Shen W, Liu Y (2011) A petrography-SIMS combined study of ^{60}Fe-^{60}Ni and ^{53}Mn-^{53}Cr in sulfides from EH3 chondrites (abstract). Meteorit & Planet Sci 46:5237
Lin Y, Gyngard F, Zinner E (2010) Isotopic analysis of supernova SiC and Si_3N_4 grains from the Qingzhen (EH3) chondrite. Astrophys J 709:1157–1173
Lin Y, Kimura M (1998) Petrographical and mineral chemical study of new EH melt rocks and a new grouplet of enstatite chondrites. Meteorit Planet Sci 33:501–511
Lin Y, Kimura M, El Goresy A (1990) Discovery of a new aqueous Fe-Cr-sulfide in some enstatite chondrites (abstract). Meteoritics 25:379
Lin Y, Kimura M, Hiyagon H, Monoi A (2003) Unusually abundant refractory inclusions from Sahara 97159 (EH3): a comparative study with other groups of chondrites. Geochim Cosmochim Acta 67:4935–4948
Lin Y, Ouyan Z, El Goresy A (2002b) FeO-rich silicates and Ca, Al-rich inclusions in Qingzhen and Yamato 691 (EH3) meteorites: Evidence for migration of mass in the solar nebula. Chin Sci Bull 47:150–153
Lin Y, Nagel H-J, Lundburg L L and El Goresy A (1991) MAC88136 - The first EL3 chondrite (abstract). Lunar and planetary science conference XXII:811–812
Lodders K, Fegley B Jr (1993) Lanthanide and actinide chemistry at high C/O ratios in the solar nebula. Earth Planet Sci Lett 117:125–145
Maruyama S, Ebisuzaki T (2017) Origin of the earth: a proposal of new model called ABEL. Geosci Front 8:253–274
McCoy TJ, Dickinson TL, Lofgren GE (1999) Partial melting of the Indarch (EH4) Meteorite: a textural, chemical and phase relations view of melting and melt migration. Meteorit Planet Sci 34:735–746

McCoy T J, Dickinson T L and Lofgren G E (1997b) Experimental and petrologic studies bearing on the origin of aubrites (abstract). NIPR symposium on Antarctic Meteorites XXII:103–105
McCoy T J, Dickinson T L and Lofgren G E (1997a) Partial melting of Indarch (EH4) from 1000–1425 C - New insights into igneous processes in enstatite meteorites (abstract). Lunar and planetary science conference XXVIII:903–904
Mezger K, Schönbächler M, Bouvier A (2020) Accretion of the earth—missing components? Space Sci Rev. https://doi.org/10.1007/s11214-020-00649-y
Moreau J, Kohout T, Wunnemann K, Halodova P, Haloda J (2019) Shock physics mesoscale modeling of shock stage 5 and 6 in ordinary and enstatite chondrites. Icarus 332:50–65
Nagel H-J, Lin Y, El Goresy A (1989) Sphalerite compositions in meteorites: a dilemma of an originally promising cosmobarometer (abstract). Meteoritics 24:307
Nittler LR, Hoppe P, Alexander CMOD, Amari S, Eberhardt P, Gao X, Lewis RS, Strebel R, Walker RM, Zinner E (1995) Silicon nitride from supernovae. Astrophys J Lett 453:L25–L28
Nittler LR, Starr RD, Weider SZ, McCoy TJ, Boynton WV, Ebel DS, Ernst CM, Evans LG, Goldsten JO, Hamara DK, Lawrence DJ, McNutt RL, Schlemm CE, Solomon SC, Sprague AL (2011) The major-element composition of Mercury's surface from MESSENGER X-ray spectrometry. Science 333:1847–1850
Patzer A, Hill D, H. and Boynton W. V. (2001) Itqiy: A metal-rich enstatite meteorite with achondritic texture. Meteorit Planet Sci 36:1495–1505
Patzer A, Schlüter J, Schultz L, Tarkian M, Hill DH, Boynton WV (2004) New findings for the equilibrated enstatite chondrite Grein 002. Meteorit Planet Sci 39:1555–1575
Piani L, Marrocchi Y, Libourel G, Tissandier L (2016) Magmatic sulfides in the porphyritic chondrules of EH enstatite chondrites. Geochim Cosmochim Acta 195:84–99
Piani L, Marrocchi Y, Rigaudier T, Vacher LG, Thomassin D, Marty B (2020) Earth's water may have been inherited from material similar to enstatite chondrite meteorites. Science 369:1110–1113
Piani L, Robert F, Beyssac O, Binet L, Bourot-Denise M, Derenne S, Le Guillou C, Marrocchi Y, Mostefaoui S, Rouzaud JN (2012) Structure, composition, and location of organic matter in the enstatite chondrite Sahara 97096 (EH3). Meteorit Planet Sci 47:8–29
Pignatale FC, Liffman K, Maddison ST, Brooks G (2016) 2D condensation model for the inner Solar Nebula: an enstatite-rich environment. Mon Not R Astron Soc 457:1359–1370
Rambaldi ER, Housley RM, Rajan RS (1984) Occurrence of oxidized components in Qingzhen enstatite chondrite. Nature 311:138–140
Rambaldi ER, Rajan RS, Housley RM, Wang D (1986) Gallium-bearing sphalerite in a metal-sulfide nodule of the Qingzhen (EH3) chondrite. Meteoritics 21:23–31
Render J, Fischer-Godde M, Burkhardt C, Kleine T (2017) The cosmic molybdenum-neodymium isotope correlation and the building material of the Earth. Geochem Perspect Lett 3:170–178
Rubin AE (1983) The Adhi Kot breccia and implications for the origin of chondrules and silica-rich clasts in enstatite chondrites. Earth Planet Sci Lett 64:201–212
Rubin AE (1997) Sinoite (Si_2N_2O): crystallization from EL chondrite impact melts. Am Miner 82:1001–1006
Rubin AE (2011) Origin of the differences in refractory-lithophile-element abundances among chondrite groups. Icarus 213:547–558
Rubin AE (2015) Impact features of enstatite-rich meteorites. Chem Erde-Geochem 75:1–28
Rubin AE, Wasson JT (2011) Shock effects in "EH6" enstatite chondrites and implications for collisional heating of the EH and EL parent asteroids. Geochim Cosmochim Acta 75:3757–3780
Van Schmus WR, Wood JA (1967) A chemical-petrologic classification for the chondritic meteorites. Geochim Cosmochim Acta 31:747–765
Sears DW, W. K. G. and Wasson J. T. (1982) The compositional classification of chondrites: II-The enstatite chondrite groups. Geochim Cosmochim Acta 46:597–608
Sears DWG, Weeks KS, Rubin AE (1984) First known EL5 chondrite-evidence for dual genetic sequence for enstatite chondrites. Nature 308:257–259
Sikdar J, Rai VK (2020) Si-Mg isotopes in enstatite chondrites and accretion of reduced planetary bodies. Sci Rep 10:1273
Skinner BJ, Luce FD (1971) Solid solutions of the type (Ca, Mg, Mn, Fe)S and their use as geothermometers for the enstatite chondrites. Am Miner 56:1269–1297
Udry A, Wilbur ZE, Rahib RR, McCubbin FM, Vander KK, E., McCoy T. J., Ziegler K., Gross J., DeFelice C., Combs L. and Turrin B. D. (2019) Reclassification of four aubrites as enstatite chondrite impact melts: potential geochemical analogs for Mercury. Meteorit Planet Sci 54:785–810
Vilas F (1985) Mercury: absence of crystalline Fe^{2+} in the regolith. Icarus 64:133–138
Warren PH (2011) Stable-isotopic anomalies and the accretionary assemblage of the Earth and Mars: a subordinate role for carbonaceous chondrites. Earth Planet Sci Lett 311:93–100
Wasson J T (1988) The building stones of the planets. In Mercury F Vilas, C R Chapman and M S Mtthews eds. Univ Arizona Press. pp. 622–653
Weisberg MK, Ebel DS, Connolly HC Jr, Kita NT, Ushikubo T (2011) Petrology and oxygen isotope compositions of chondrules in E3 chondrites. Geochim Cosmochim Acta 75:6556–6569
Weisberg MK, Kimura M (2012) The unequilibrated enstatite chondrites. Chem Erde 72:101–115
Weisberg MK, Prinz M, Fogel RA (1994) The evolution of enstatite and chondrules in unequilibrated enstatite chondrites: Evidence from iron-rich pyroxene. Meteoritics 29:362–373
Weyrauch M, Horstmann M, Bischoff A (2018) Chemical variations of sulfides and metal in enstatite chondrites—Introduction of a new classification scheme. Meteorit Planet Sci 53:394–415
Xu Y, Gu L, Li Y, Mo B, Lin Y (2018) Combination of focused ion beam (FIB) and microtome by ultrathin slice preparation for transmission electron microscopy (TEM) observation. Earth, Planets and Space 70:150
Xu Y, Lin Y, Zhang J, Hao J (2016) The first discovery of presolar graphite grains from the highly reducing Qingzhen (EH3) meteorite. Astrophys J 825:111
Zhang Y, Benoit PH, Sears DWG (1995) The classification and complex thermal history of the enstatite chondrites. J Geophys Res 100:9417–9438
Zhao X, Bose M, Floss C, Stadermann FJ, Lin Y (2010) Investigation of presolar silicate grains from enstatite chondrites (abstract). Meteorit Planet Sci Suppl 73:5254
Zhao C, Lodders K, Bloom H, Chen H, Tian Z, Koefoed P, Peto MK, Wang K (2020) Potassium isotopic compositions of enstatite meteorites. Meteorit Planet Sci 55:1404–1417
Zhu K, Moynier F, Schiller M, Bizzarro M (2020) Dating and tracing the origin of enstatite chondrite chondrules with Cr Isotopes. Astrophys J Lett 894:L26
Zinner E, Amari S, Guinness R, Jennings C, Mertz AF, Nguyen AN, Gallino R, Hoppe P, Lugaro M, Nittler LR, Lewis RS (2007) NanoSIMS isotopic analysis of small presolar grains: search for Si_3N_4 grains from AGB stars and Al and Ti isotopic compositions of rare presolar SiC grains. Geochim Cosmochim Acta 71:4786–4813

Publisher's Note